Electronic Supplementary Material (ESI) for Journal of Materials Chemistry C.
This journal is © The Royal Society of Chemistry 2020

Supporting Information

for

Resistive switching performance of fibrous crosspoint memories based on organic-inorganic halide perovskite

Pan Shu,[a] Xiaofei Cao,[a] Yongqiang Du,[a] Jiankui Zhou,[a] Jianjun Zhou,[a] Shengang Xu,[ab] Yingliang Liu,*[ab] and Shaokui Cao,*[ab]

[a] School of Materials Science and Engineering, Zhengzhou University, Zhengzhou 450001, People's Republic of China

[b] Henan Key Laboratory of Advanced Nylon Materials and Application, Zhengzhou University, Zhengzhou 450001, People's Republic of China.

RRAM test method

Fig. S1a shows the digital photograph of *FCPe*-RRAM device with an architecture of Al@$MAPbI_3$/Al on a home-made test holder, which is made of stainless steel. Four pillars on the test holder are wound with the insulating PTFE film to prevent the current leakage. The functional RS fiber of Al@$MAPbI_3$ is perpendicularly placed on the bare Al fiber as the top electrode at a certain bending angle. The bare Al fiber

serves as the bottom electrode. Thereby, the *FCPe*-RRAM devices with different bending angle are obtained in the form of (±V) Al@$MAPbI_3$/Al (⏚). In the RRAM test process, the voltage is applied on the Al fiber of functional RS fiber (Al@$MAPbI_3$). The bare Al fiber on the bottom is used as a ground wire. The current-voltage (I−V) characteristics are tested under a direct current (DC). The voltage sweep is generally started from a positive bias voltage, such as 0 V → 4 V → 0 V → −4 V → 0 V, while the compliance current (I_{cc}) of 100 mA is applied to safeguard the semiconductor analyzer. The different bending angles, such as 0°, 15°, 30° or 45°, are set through the upward or downward movement of Al electrodes on the insulating pillars. The calculation process of bending angles is shown in **Fig. S1b.**

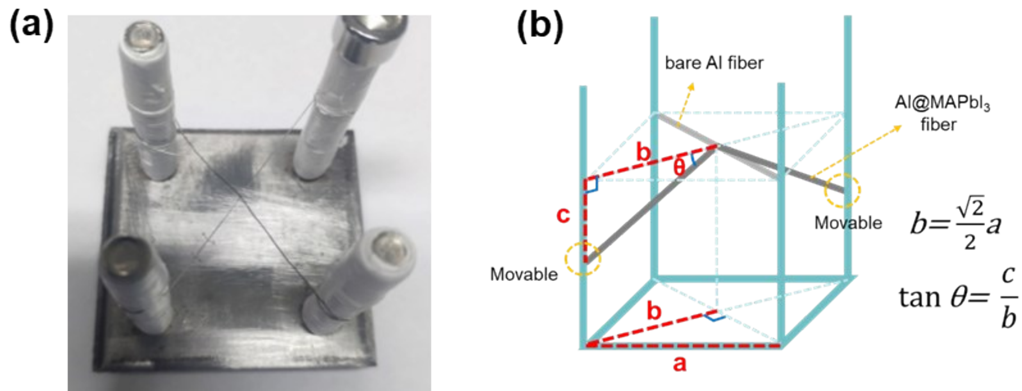

Fig. S1 The digital photograph of *FCPe*-RRAM device with an architecture of Al@$MAPbI_3$/Al (a); The calculation process of bending angles (b);

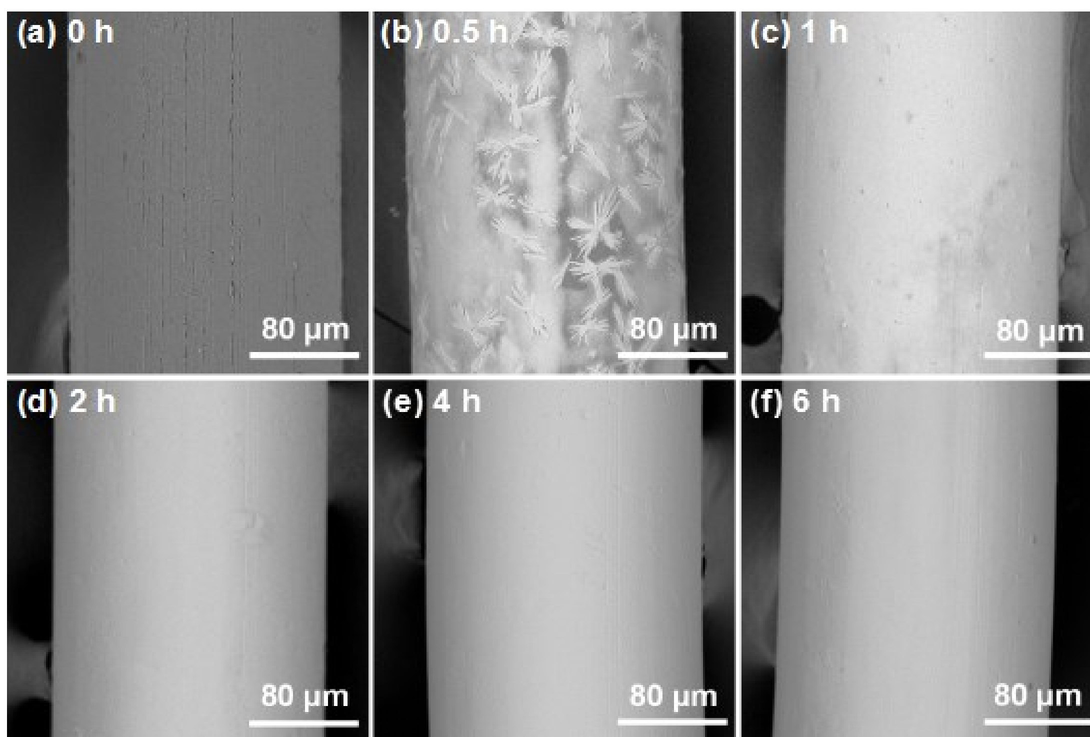

Fig. S2 Top-view SEM images of $MAPbI_3$ perovskite films being fabricated at different dip-coating time (a: 0 h; b: 0.5 h; c: 1 h; d: 2 h; e: 4 h; f: 6 h).

Dip-coating time

The SEM images in **Fig. S2** show how the dip-coating time in the precursor solution (1.0M) with the anti-solvent processing of ethyl acetate affects the perovskite morphology. Evidently, with the increase of dip-coating time, the coverage ratio of $MAPbI_3$ on the Al fiber is increased gradually. At the 2-hour dip-coating time, the $MAPbI_3$ perovskite has completely covered the Al surface, presenting a compact and uniform perovskite film.

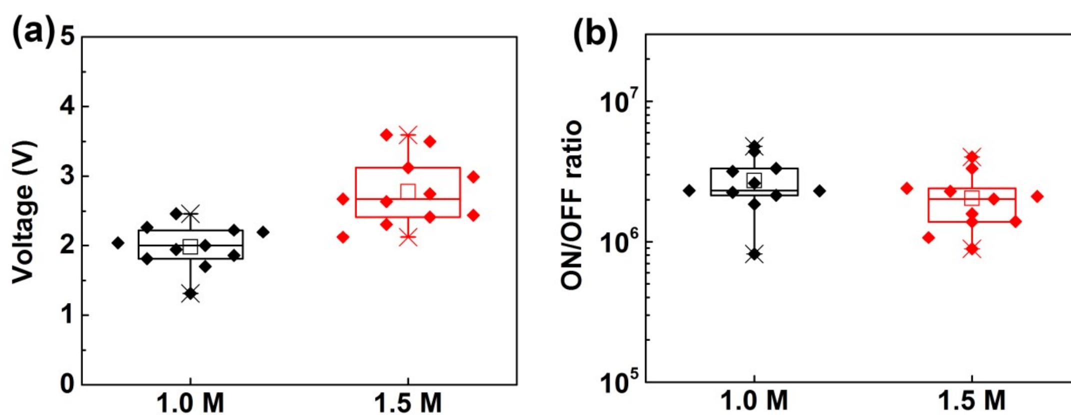

Fig. S3 The box-whisker distributions of SET voltage (a) and ON/OFF ratio (b) derived from 11 *FCPe*-RRAM devices with different precursor solution concentrations.

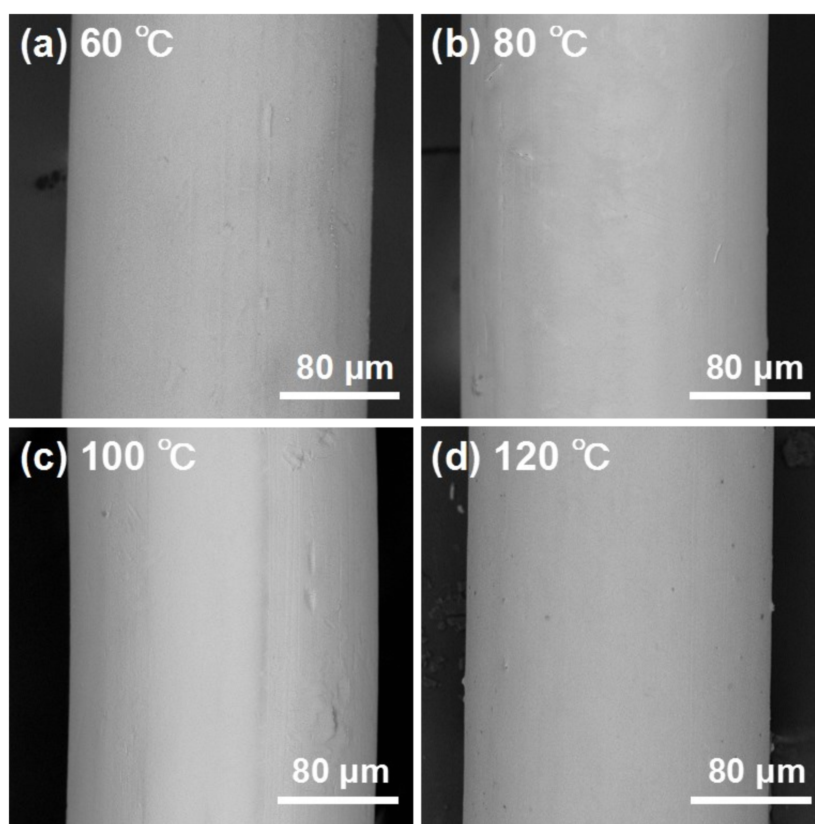

Fig. S4 Top-view SEM images of $MAPbI_3$ perovskite films being annealed at different temperatures (a: 60 °C; b: 80 °C; c: 100 °C; d: 120 °C).

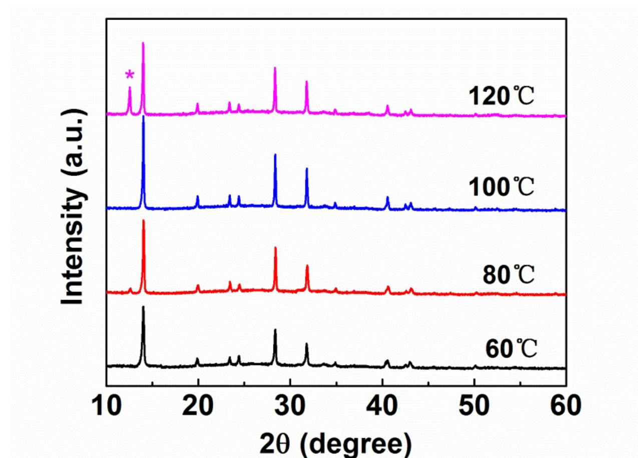

Fig. S5 XRD patterns of $MAPbI_3$ perovskite films being annealed at different temperatures, in which the peak of PbI_2 is marked by *.

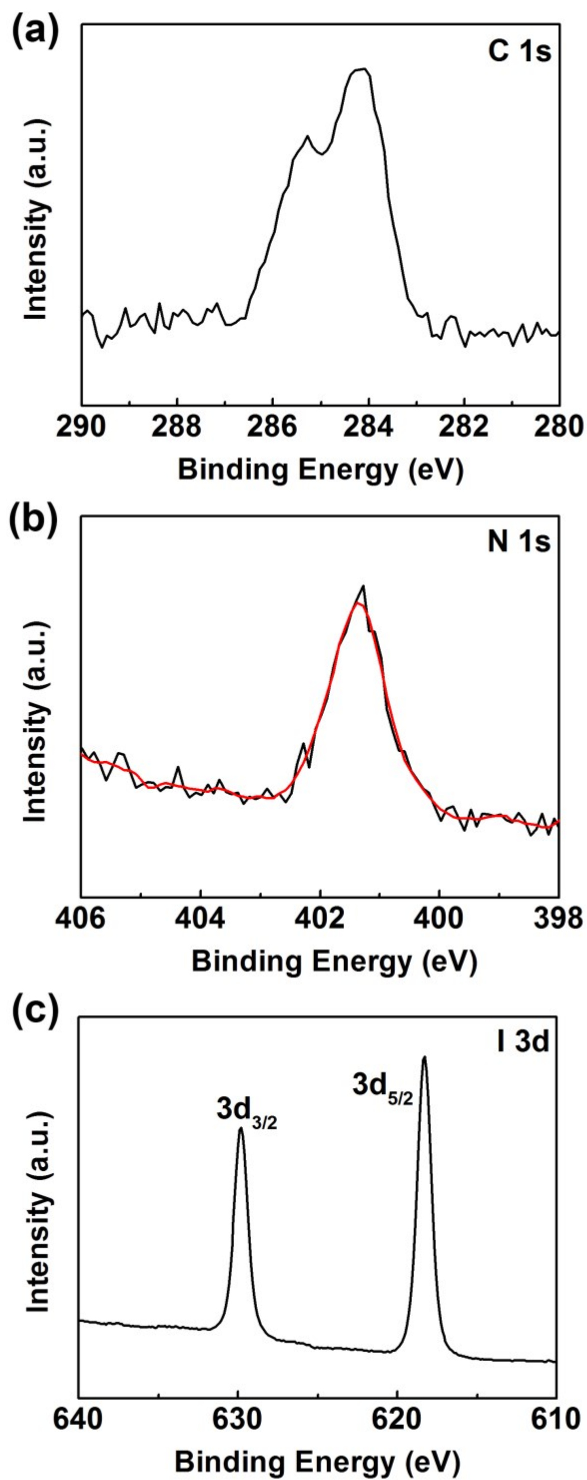

Fig. S6 High-resolved XPS spectra (a, C 1s; b, N 1s; c, I 3d).

The C 1s signal has been splitted into two peaks due to the interference of the

carbon contamination including CO_2 and organic carbon in the chamber, which is also responsible for high carbon content. The N 1s signal is located at the binding energy of 401.3 eV. In addition, the double peaks of I 3d at the binding energy of 142.6 eV and 137.7 eV correspond to I $3d_{3/2}$ and I $3d_{5/2}$.

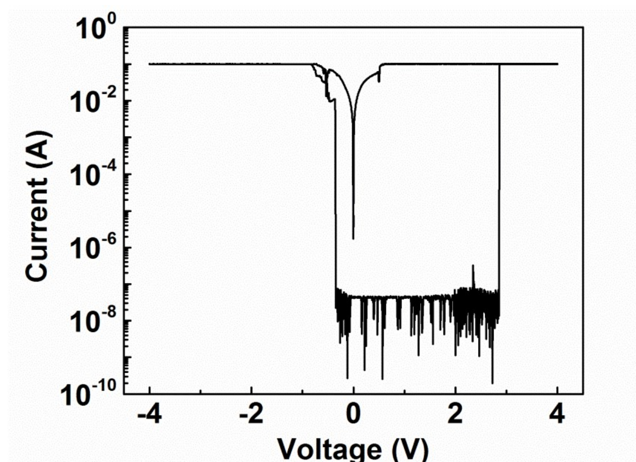

Fig. S7 I−V curve of Al/$MAPbI_3$@Al device using a forward voltage sweep of 0 V → 4 V → 0 V → −4 V → 0 V.

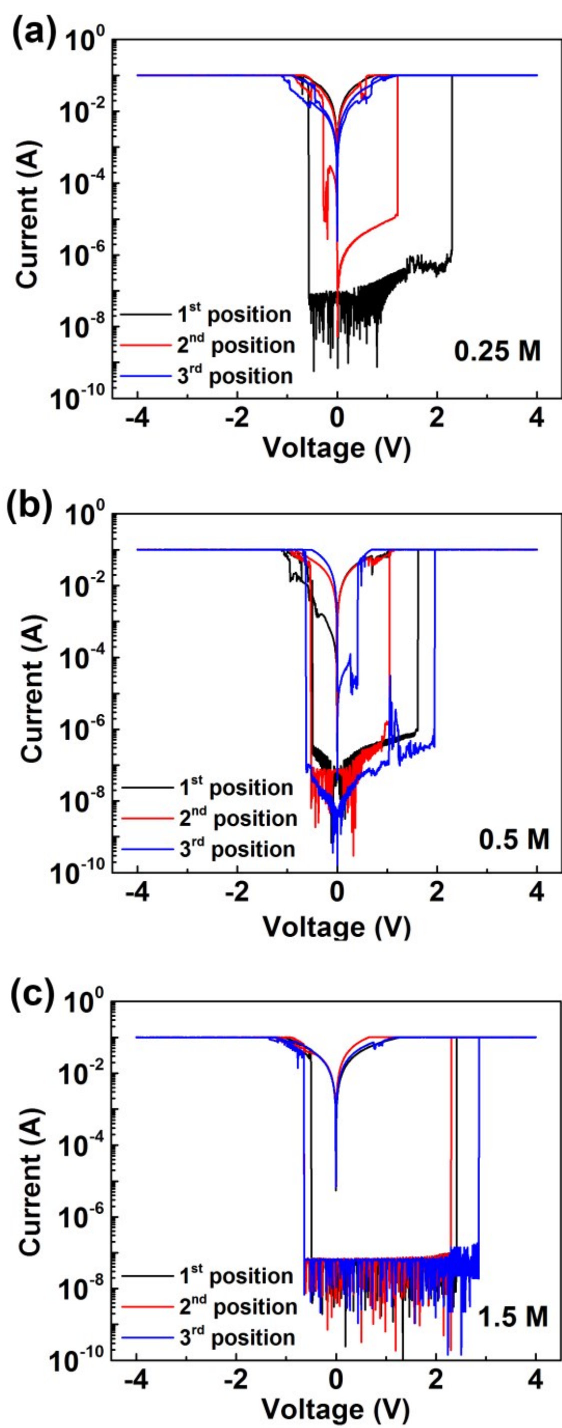

Fig. S8 I−V curves on the random locations of *FCPe*-RRAM devices (a, 0.25 mol/L; b, 0.5 mol/L; c, 1.5 mol/L).

This is to demonstrate the feasibility to put this crosspoint structure into a crossbar array for wearable electronic devices. When the contact position between the fibers is moved due to separation and reattachment, the RS characteristic can remain at the new position. When the precursor solution concentration is 0.25 mol/L or 0.5 mol/L, the unstable RS characteristics appear in different locations due to the incomplete coverage of perovskite film on the Al fiber. However, the results indicate that the good reproducibility of RS characteristics is achieved when the perovskite film is dip-coated with the precursor solution of 1.0 mol/L and 1.5 mol/L.

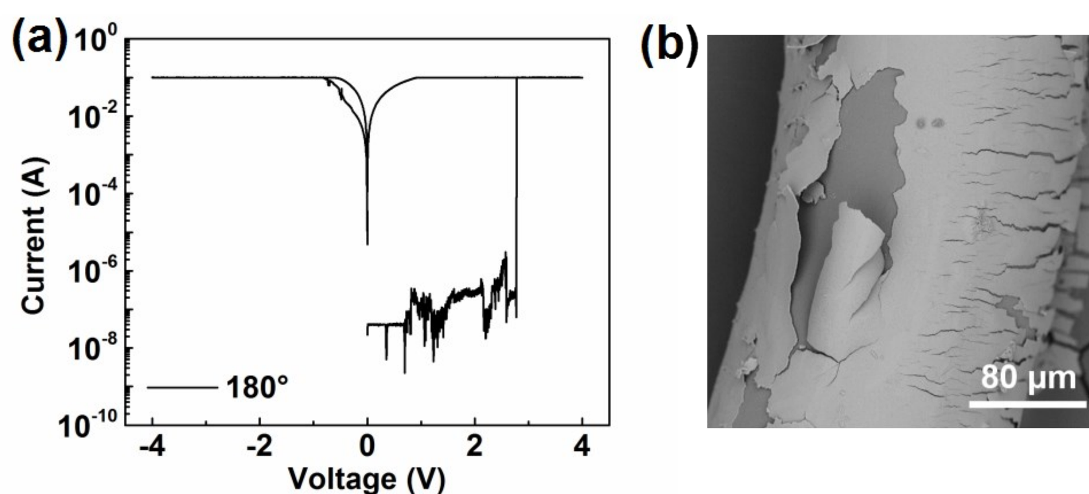

Fig. S9 I−V curve of *FCPe*-RRAM device at a bending angle of 180° (a); Top-view SEM image of $MAPbI_3$ perovskite film at a bending angle of 180° (b).

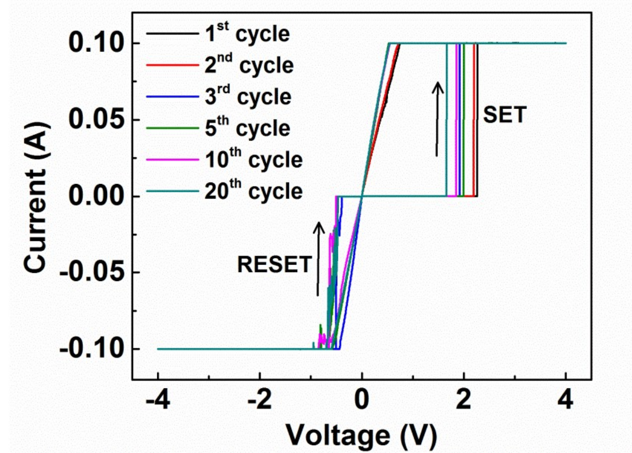

Fig. S10 The linear I−V curves of *FCPe*-RRAM device for 20 sweeps.

Table S1. A brief comparison of different fiber-shaped memory devices.

RS Materials	SET/RESET voltage (V)	ON/OFF ratio	Device type[a]	Fabrication method	References
CuO	+2.4/−2.2	~10^2	WMRM	Thermal oxidation	S1
GO	+3.5	~10^6	WORM	CVD	S2
rGO	+5.8/−5.8	~10^9	WMRM	CVD	S3
Bi_2Se_3	−1.2/+0.7	~10^5	WMRM	Microwave synthesis	S4
$MAPbCl_xI_{3-x}$	+1.00/−1.58	~20	WMRM	Dip-coating	S5
Al_2O_3	−2.0/+1.0	~10^2	WMRM	Native oxidation	S6
$MAPbI_3$	+1.66/−0.47	~10^6	WMRM	Dip-coating	This work

[a] WMRM is the abbreviation for write-many-times-read-many-times; WORM is the abbreviation for write-once-read-many-times.

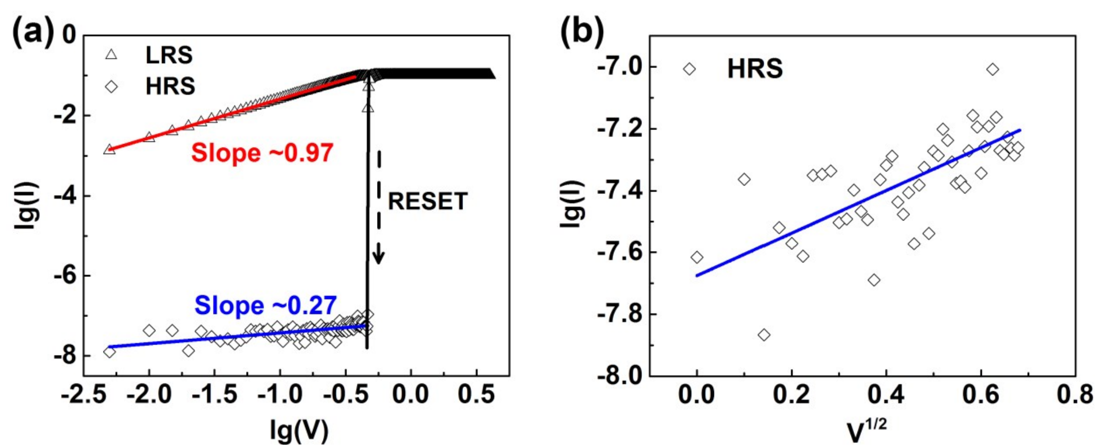

Fig. S11 Double-logarithm I–V plots of *FCPe*-RRAM device in the RESET process (a) and lgI–$V^{1/2}$ plots at the HRS state in the RESET process (b).

References:

S1. J.-W. Han and M. Meyyappan, *AIP Adv.*, 2011, **1**, 032162.

S2. G. Sun, J. Liu, L. Zheng, W. Huang and H. Zhang, *Angew. Chem. Int. Ed.*, 2013, **52**, 13351-13355.

S3. R. Li, R. Sun, Y. Sun, P. Gao, Y. Zhang, Z. Zeng and Q. Li, *Phys. Chem. Chem. Phys.*, 2015, **17**, 7104-7108.

S4. X. Y. Zhang, F. S. Wen, J. Y. Xiang, X. C. Wang, L. M. Wang, W. T. Hu and Z. Y. Liu, *Appl. Phys. Lett.*, 2015, **107**, 103109.

S5. K. Yan, B. Chen, H. Hu, S. Chen, B. Dong, X. Gao, X. Xiao, J. Zhou and D. Zou, *Adv. Electron. Mater.*, 2016, **2**, 1600160.

S6. A. Jo, Y. Seo, M. Ko, C. Kim, H. Kim, S. Nam, H. Choi, C. S. Hwang and M. J. Lee, *Adv. Funct. Mater.*, 2017, **27**, 1605593.